Synthesis, Structure, and Thermo-Physical Properties of $Fe_2O_3.Al_2O_3$ and Polyethylene Nanocomposites

Amir Reza Vakhshouri, Akif Azizov, Reyhan Aliyeva, Shefeq Bagirova

Institute of Petrochemical Processes, Azerbaijan National Academy of Sciences, AZ1025, Baku, Republic of Azerbaijan

Received 15 August 2011; accepted 20 September 2011
DOI 10.1002/app.35661
Published online 12 December 2011 in Wiley Online Library (wileyonlinelibrary.com).

ABSTRACT: In this study, $Fe_2O_3.Al_2O_3$/polyethylene composites were prepared using a two-step process. In the first step, PE is synthesized using titanium based metallocene catalyst system. While the synthesized PE was subsequently purified, hydrated alumina filled PE (MHFP) composites was formed by the hydrolysis of methylaluminoxane (MAO). In the second step, $Fe_2O_3.Al_2O_3$/PE was prepared via thermal decomposition of ferric formate in a high temperature solution of MHFP composite. The structure, morphology, and thermal properties of the composites were characterized using the XRD, FTIR, SEM-EDX, TGA, and DSC analytical techniques. Results showed that the incorporation of a suitable amount of $Fe_2O_3.Al_2O_3$ into the composites enhances the thermal stability. © 2011 Wiley Periodicals, Inc. J Appl Polym Sci 124: 5106–5112, 2012

Key words: composites; PE; iron (III) oxide; aluminum oxide; thermo-physical properties; morphology; DSC

INTRODUCTION

Production of polymer composites consists of components. Composites provide the useful properties of both matrix and reinforcing component, including thermal stability, desirable physical, mechanical, and rheological properties. Thermal and electrical conductivity are two important properties that composites may offer.[1–7] The great interest in polymer composites containing metallic (e.g., metals, metal oxides, and metal complexes) nanoparticles or clusters are motivated by the wide applications of these materials from polymeric catalysts systems to nanoelectronics application.

Metal containing nanoparticles can be prepared by a variety of methods: thermal, ion-beam, or plasma evaporation, followed by condensation and co-condensation, and electric-spark, galvanic, or mechanochemical dispersion techniques.[8,9] For example, Fe_2O_3 particles were prepared by oxidation of Fe-containing particles,[10] by a micro-emulsion method,[11] and in a sol–gel process.[12] The composition and structure of nanoparticles were shown to be strongly dependent on the preparation procedure. Thermal decomposition of iron (III) organic salts is a well-known method of preparing fine iron oxide nanoparticles.[13,14]

In this work, iron (III) formate was decomposed by adding the solution dropwise to a hydrophobic medium. Subsequently, the drops were transferred to a nanoreactor where the solvent evaporation, thermal decomposition, and nucleation occurred, without supply of any additional substance. This is a specific feature of the process used in this work to produce a material containing Fe_2O_3 particles. The preparation and investigation of iron (III) oxide nanoparticles were reported elsewhere.[11–15] In this work, a procedure for embedding iron (III) oxide and alumina particles in a PE matrix via methylaluminoxane (MAO) hydrolyzing[16,17] and ferric formate decomposition was developed to examine their structures and to study the particles–matrix interaction.

EXPERIMENTAL

Materials

Ethylene produced at the EP-300 plant in Sumgait, Azerbaijan, was purified and dried over freshly calcined aluminum oxide. The ethylene content (no less than 99.9%) was measured with a gas–liquid chromatography (CHROM-5) equipped with flame-ionization detectors and a 2-m long column packed with 10% Apiezon. Cocatalyst methylaluminoxane (MAO) (Aldrich) was used as a 10% solution in toluene (d = 0.875 g/cm^3 and T_b = 111°C). Metallocene type of catalyst included Cp_2TiCl_2 from TCI-EP (Japan), $AlEt_2Cl$, MAO, solvents (n-hexane, toluene, benzene, and ethanol) and ferric formate from Sigma-Aldrich (St. Louis, MO) were used as received.

Preparation of hydrated alumina filled PE

The polymerization of ethylene was performed in a 200-cm^3 stainless steel autoclave designed for a

Correspondence to: A. R. Vakhshouri (amir.rv@live.com).

pressure of 5 MPa. The temperature was maintained constant during the reaction by an ultra-thermostat and measured by a thermocouple connected to a recording device. The autoclave was equipped with a stirrer, a jacket for cooling or heating, and pipes for loading components, including the solvents and the aluminum organic compound. The pressure in the reactor and in the initial cylinder was measured with a manometer. Before the process, the reactor was connected to the vacuum setup at 65–70°C for 1–2 h to evacuate the oxygen and moisture and then dry argon was fed into the reactor. The polymerization of ethylene was performed in toluene. All operations were performed under a flow of argon. Components of the reaction mixture were charged in the reactor in the following order: 5 mg Cp_2TiCl_2 as catalyst, 3 ml of $AlEt_2Cl$ (30% solution in toluene), and 4 ml MAO (10% solution in toluene) mixture as co-catalysts and the residual amount of the solvent. After stirring at room temperature (20–22°C) for 15–20 min, ethylene was fed to the reactor while stirring. The ethylene pressure was controlled by a manometer. The initial pressure was 6 atm; after 3–4 minutes, the pressure fell strongly due to contact of ethylene with the catalyst surface, and then the pressure decrease occurred slowly. After 25–30 min, when the pressure became constant the polymerization stopped. Then, the active catalyst was decomposed by adding a 10% ethanol solution of HCl. The polymer was filtered off and washed with acidified ethanol and distilled water. After washing and filtration, the polymer was dried under vacuum at 60–70°C. The next step of PE purification needed a high concentration of HCl, ethanol, and a large amount of *n*-hexane. After conducting this step, the particles of aluminum inorganic compounds, especially hydrated alumina, which remained from hydrolyses of the MAO, embedded in the PE matrix. The aluminum compounds were about 5–20% of the product weight.[16,17]

Preparation of $Fe_2O_3.Al_2O_3$/PE nanocomposites

For the preparation of $Fe_2O_3.Al_2O_3$/PE nanocomposite, first the sample of hydrated alumina filled PE was put in the bobbin oil then stirred to prepare the solution. The solution of $Fe(HCOO)_3$ in benzene was added to the blend under flowing inert gas. The flow rate of inert gas was adjusted so that it rapidly removed the ligands and solvent from the reactor. Temperature was set at 200°C. $Fe(HCOO)_3$ decomposed to Fe_2O_3 at the elevated temperature. On the other hand, hydrated alumina lost a large amount of H_2O. After blending, the final product was washed with *n*-hexane to remove the residual oil, then it was filtrated and the resultant powder was dried under vacuum and stored in the air atmosphere. The product was dark red. Three ratios of the $Fe_2O_3.Al_2O_3$/PE (FAFP) were prepared for the characterization (Table I).

TABLE I
The Samples Identifications and Compositions

	Composition		
Samples	Fe_2O_3 wt %	Al_2O_3 wt %	PE wt %
FAFP1	~ 3%	~ 10%	87%
FAFP2	~ 2%	~ 10%	88%
FAFP3	~ 1%	~ 10%	89%

Characterization

The structures of the composites were investigated by powder X-ray diffraction (XRD). The experiments were carried out with a Siemens D5000 instrument. Scattering patterns were obtained with Cu Kα radiation at a rate of 2°/min. XRD scans were recorded from 4 to 70° for 2θ with a 0.020° step-width and 0.3 s step time at room temperature. The XRD data were analyzed using the DIFFRAC-Plus program (Siemens, Germany), and the patterns were identified using the ICDD PDFMaint computer reference database. Fourier-transform infrared (FTIR) spectra were obtained using a Bruker Tensor 27 spectrometer for characterization of the composites at room temperature.

Scanning electronic microscopy (SEM) was used to characterize the composites morphologies. The composites specimens were broken in liquid nitrogen and the fractured surfaces were coated with gold (thickness, 15 nm), before SEM investigations. SEM images were obtained using a S360 SEM microscope. The SEM-EDX was used to determine the elements. The sample was coated with 15 nm gold. Copper was used as optimization element. The tilt, elevation, and azimuth degrees were 0.0, 35.0, and 0.0, respectively. The magnification and accelerating voltage were 1000 and 20 kV, respectively, the process time set to 2.

Thermal gravimetric analyses (TGA) were carried out by using a TGA-PL thermo-analyzer instrument in the range of 25–600°C with a linear heating rate of 10°C/min under nitrogen. The nitrogen flow was 50 ml/min. Samples were examined in a sealed platinum pan.

Differential scanning calorimetry (DSC) examination was performed in air atmospheres using a DT-50 thermal analyzer in the range of 20–550°C with a linear heating rate of 15°C/min, maintained at 200°C for 1 min to remove thermal history. The air flow rate was 30 ml/min. The precision of the calorimeter and temperature measurements were ±2.0% and ±2.0°C, respectively. Samples were examined in a

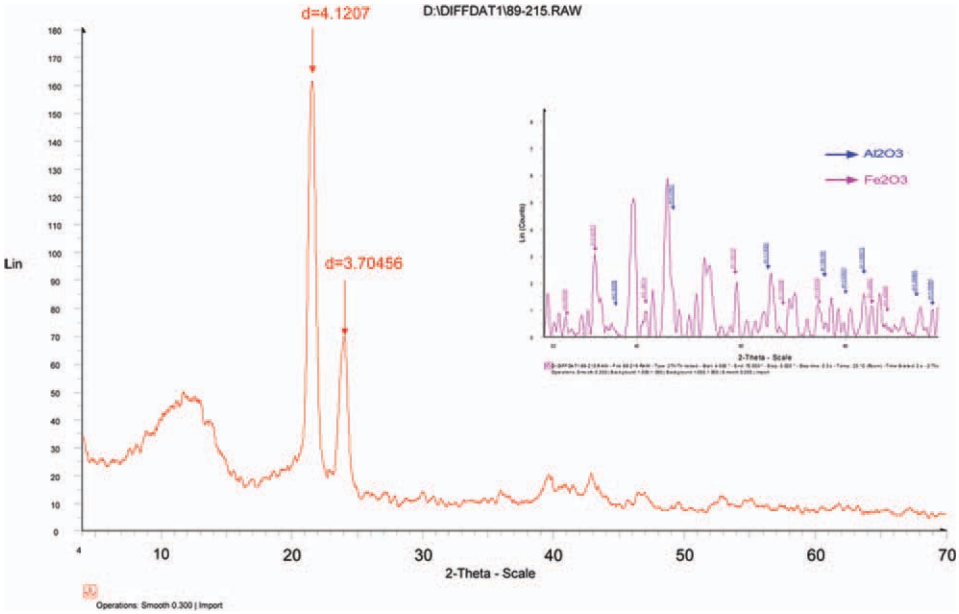

Figure 1 XRD spectrum of FAFP1 at 2θ = 0–70 and magnification of peaks at 2θ = 30–70. [Color figure can be viewed in the online issue, which is available at wileyonlinelibrary.com.]

sealed platinum pan with a sample mass of about 10 mg. Thermal properties, melting temperature, and enthalpy of melting were determined from the DSC thermograms. The latent heat values were calculated as the total area under the melting peaks of PE in the composites by the thermal analysis software.

RESULTS AND DISCUSSION

Structure and morphology of composites

X ray diffraction (XRD)

Figure 1 shows the XRD spectrum of FAFP1 which indicates an amorphous peak of PE at diffraction angle of about 20° and two crystalline peaks at diffraction angles of 21.67° and 24.04°. In fact, PE crystallizes in an orthorhombic crystalline structure with lattice dimensions of $a = 7.40$ Å, $b = 4.93$ Å, and $c = 2.534$ Å. The c-direction is the chain direction.[18] Beside these sharp peaks, new small peaks were observed. These peaks, corresponding to Al and Fe compounds, were compared with various pattern peaks. The calculated d-spacings for related alumina were 3.46, 2.54, 2.37, 2.08, 1.74, 1.59, 1.49, 1.39, and 1.36, respectively and for ferric oxide, 3.67, 2.69, 2.49, 2.20, 1.84, 1.69, 1.60, 1.48, and 1.45, respectively. These values are in agreement with the standard XRD pattern of α-Al_2O_3-Rhombohedral (PDF card #01-1243) and α-Fe_2O_3 (PDF card #33-0664). This indicates that the dark reddish brown iron oxide particles are α-Fe_2O_3.[18,19] The average particle size (D) was estimated from the Debye–Scherrer equation [eq. (1)].

$$D = K\lambda/\beta\cos\theta_\beta \quad (1)$$

Here, K is a dimensionless constant that may vary from 0.89 to 1.39, depending on the specific geometry of the scattering objects. For a perfect two-dimensional lattice, where every point on the lattice emits a spherical wave, numerical calculations yield the lower bound of 0.89 for K. β is the full width at half-maximum of peak (FWHM) in radians, and λ equals to 0.15406 nm for the wavelength of Cu Kα radiation.[20,21] The average particle sizes of Fe_2O_3 were calculated about 26 nm.

Fourier-transform infrared spectroscopy

Figure 2 displays the FTIR spectra of clean PE, MHFP, and FAFP3. All spectra have the characteristic bands of 2921 cm^{-1} and 2850 cm^{-1}, corresponding to the asymmetric and symmetric stretching vibration of C—H, respectively, 1742 cm^{-1} corresponding to the stretching vibration of C=O, 1468 cm^{-1} (CH_2 or CH_3 deformation vibration), and 720 cm^{-1} (CH_2 rocking vibration of $(CH_2)_n$, $n = 4$).[22,23] The general range of 3600–3100 cm^{-1} relating to asymmetric and symmetric OH stretching may be assigned to the water of hydration. Hydrates also absorb in the region 1670–1600 cm^{-1} relating to the distortion vibration of O—H bending. This clearly indicates that many OH groups are on the surface of the metal oxides particles because of their intense absorption effect. Besides these bands, the FAFPs have the characteristic bands of alumina and Fe_2O_3.

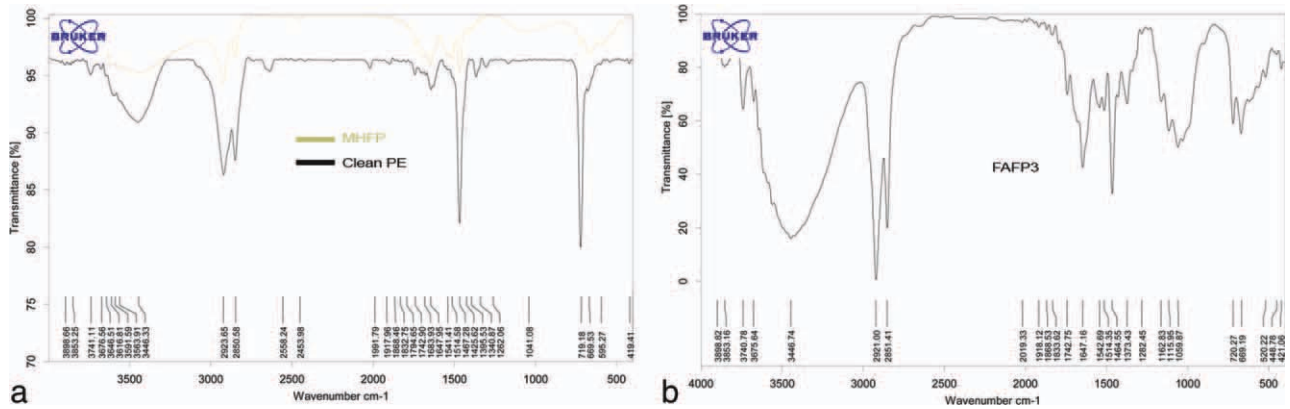

Figure 2 The FTIR spectra of clean PE, MHFP (a), and FAFP3 (b). [Color figure can be viewed in the online issue, which is available at wileyonlinelibrary.com.]

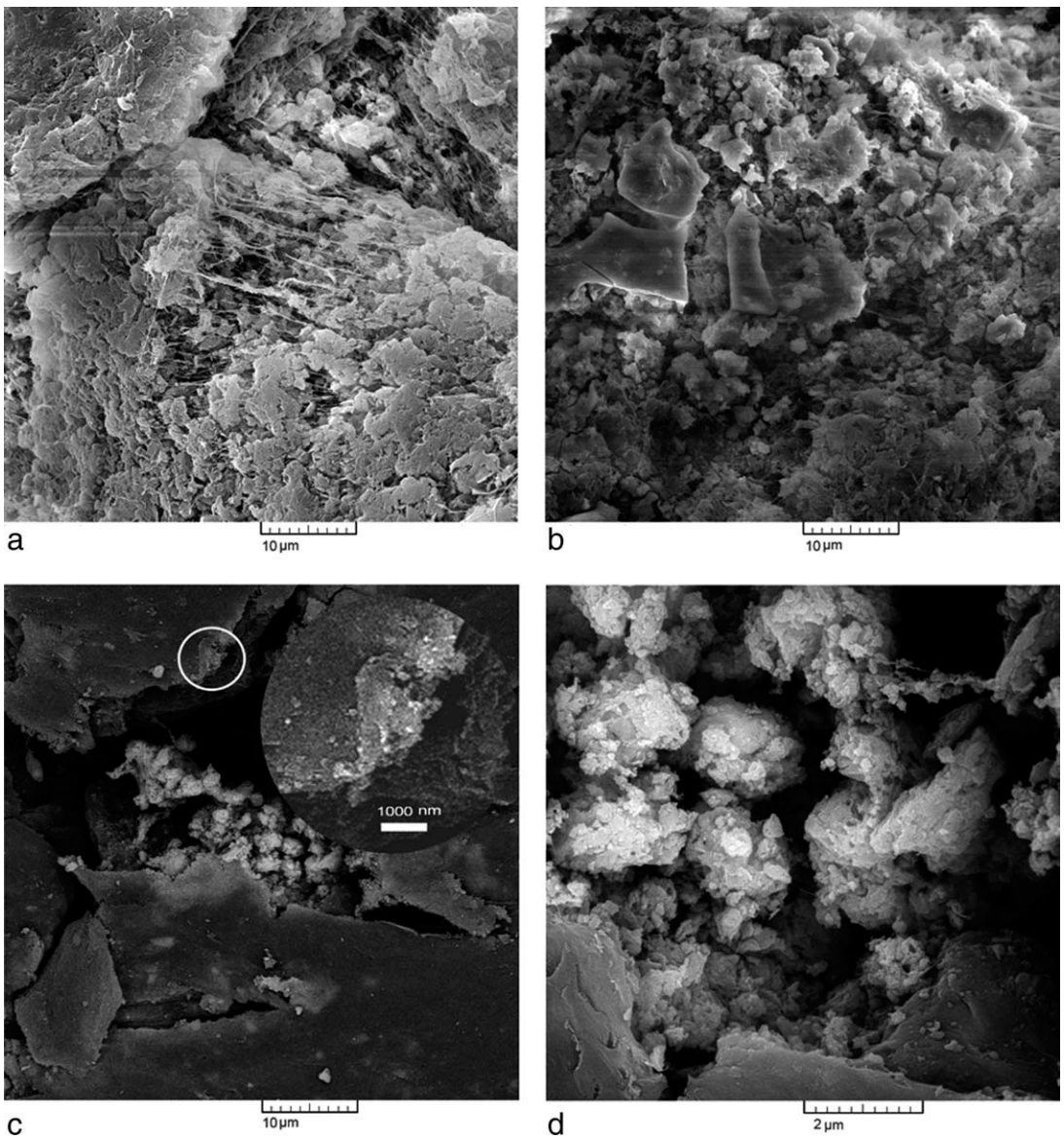

Figure 3 SEM images of the clean PE (a), MHFP (b), and FAFP1 (c–d); the inset in (c) shows higher magnification image of the highlighted circle.

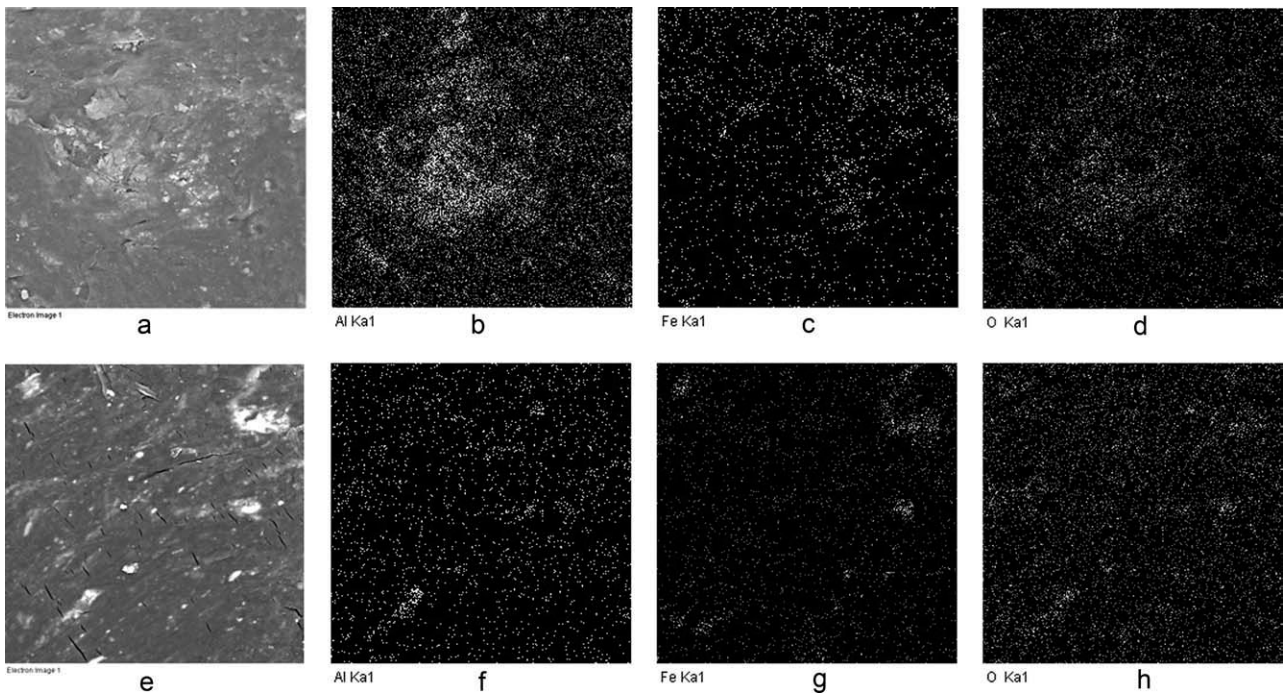

Figure 4 EPMA elemental mapping and corresponding SEM images of the FAFP1 (a–d) and FAFP2 (e–h).

The peak at 3446 cm^{-1} corresponds to the OH stretching frequency of AlO(OH), which clearly indicates that OH groups are on the surface of the alumina particles because of their strong absorption effect. The bands at 1080–880 cm^{-1} and at 550–450 cm^{-1} correspond to the stretching vibration of Al–O and Fe–O, respectively. The FTIR spectra of other composites (with 3 and 6 wt % Fe_2O_3) showed similar absorption peaks without much variation in stretching frequencies.[16,24–27]

Scanning electron microscopy and energy dispersive X-ray analysis

The morphology and the elemental composition of samples were examined by SEM-EDX method. The SEM images of clean PE, MHFP, and FAFPs are shown in Figure 3. Figure 3(b) indicates that the hydrated alumina was dispersed with various particle sizes in the composite structure. Figure 3(c,d) show random dispersions of the Fe_2O_3 particles in

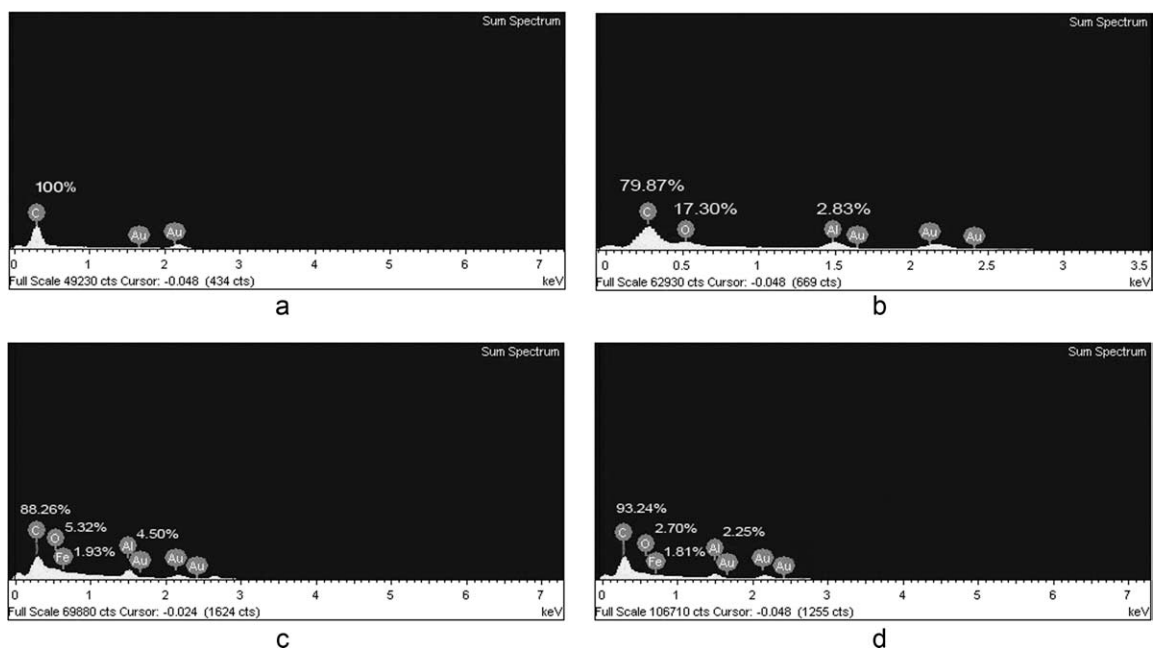

Figure 5 EDX sum spectrum results of the clean PE (a), MHFP (b), FAFP1 (c), and FAFP2 (d).

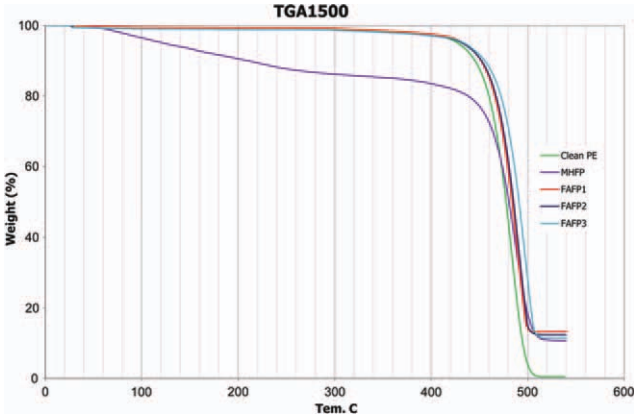

Figure 6 TGA curves of clean PE, MHFP, FAFP1, FAFP2, and FAFP3. [Color figure can be viewed in the online issue, which is available at wileyonlinelibrary.com.]

the PE matrix, where the alumina particles tend to form bigger agglomerates. Figure 3(c) also shows a big cluster of Al_2O_3 particles that are focused in Figure 3(d). In Figure 3(c) the inset shows greater magnification image of the highlighted circle, which includes Fe_2O_3 nanoparticles. We estimated from these images that the particle sizes of Al_2O_3 and Fe_2O_3 were in the ranges of 100–1500 nm and 20–200 nm, respectively. The difference in Fe_2O_3 particle sizes between SEM results (20–200 nm) and XRD analysis (26 nm) indicates that some smaller particles may be agglomerated to form Fe_2O_3 clusters because of the intermolecular interactions.

Figure 4 shows the electron probe microanalysis (EPMA) elemental mapping of FAFP1 and FAFP2. It is evident from Figure 4(c,g) that the dispersion of the Fe_2O_3 particles in the PE matrix is more homogeneous than Al_2O_3, because of their smaller particle size.

Figure 5 shows the sum spectrum of elements resulted by EDX method. The percentage of elements confirmed that the particles indeed contain hydrated alumina particles in the MHFP and Al_2O_3–Fe_2O_3 particles in the FAFPs. Note that the percentage of each element obtained by EDX can only provide a qualitative indication of the existence of the element and cannot be used for quantitative calculation because of uncertainty in the experiments.[19,28]

Thermal properties of composites

Thermogravimetric analyses

Figure 6 shows the TGA curves of the clean PE, MHFP, and FAFPs. The weight-loss data obtained from the TGA curves with respect to the temperature is shown in Table II. It can be seen from the TGA curves that there is a one-step degradation process in all samples. Happening from about 400–500°C, this step may be assigned to the degradation of the PE main chains. The weight loss for FAFPs starts obviously at higher temperature than that of pure PE.

TABLE 2
TGA Data of Samples

Samples	$T_{-15\ wt\%}$ (°C)	$T_{-50\ wt\%}$ (°C)	$T_{-70\ wt\%}$ (°C)	$T_{-85\ wt\%}$ (°C)	Residue (540°C) %
Clean PE	453	477	485	493	0.4
MHFP	367	480	493	503	10.1
FAFP1	459	483	492	499	13.7
FAFP2	461	485	495	500	12.4
FAFP3	467	490	502	506	11.1

The lower onset temperature for MHFP was as a result of water loss. $Al(OH)_3$ is known to decompose endothermically upon heating, producing H_2O and Al_2O_3. Because of the endothermic nature of the reaction, metal hydroxide absorbs the heat from the polymer and delays the thermal degradation of PE. The appearance of excessive weight loss might be due to the excessive loss of water rather than decomposition of the polymer itself. In contrast, in the FAFPs, the Al_2O_3 particles improved thermal stability of PE.[29] The results show that the thermal stability of the composites increases with increasing in Al_2O_3/Fe_2O_3 ratio.

Differential scanning calorimetry

Thermal oxidation behavior of the PE and FAFPs, under atmospheric conditions in the temperature range of 15–550°C was studied. The DSC curves of thermo-oxidation for clean PE, FAFP1, FAFP2, and FAFP3 are shown in Figure 7. The results obtained from DSC analyses of PE and composites are summarized in Table III. In the FAFPs, the melting temperature of PE increased with an increase in Fe_2O_3 content, which can be attributed to the formation of crystallites as a result of the miscibility of the

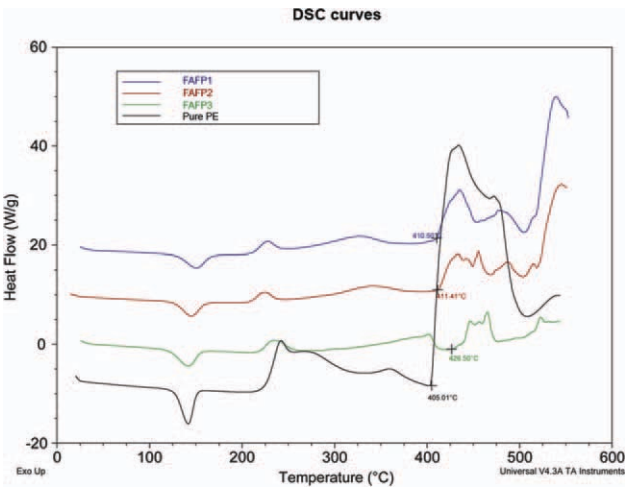

Figure 7 The DSC curves of clean PE, FAFP1, FAFP2, and FAFP3 under air atmosphere. [Color figure can be viewed in the online issue, which is available at wileyonlinelibrary.com.]

TABLE 3
The Parameters of Clean PE, FPE, FAFP1, FAFP2, and FAFP3 Obtained from DSC Measurements Under Air Atmosphere

			Thermo-oxidation main peaks (°C)			
Sample	$T_{m\text{-peak}}$ (°C)	ΔH_m (J/g)	1st peak	2nd peak	Major peak	Major 2nd peak
PE	142	241.3	241.7	360.9	424.4	532
FAFP1	150.5	161	227.6	327.4	434.5	536
FAFP2	144.8	162	223.9	339.2	432.6	537.7
FAFP3	142	167	234.9	349.1	445.3	542.6

components in the molten state. The total specific enthalpy of melting was evaluated by the use of a linear baseline over a broad thermal interval. The melting latent heat of all the blends decreased with an increase in Fe_2O_3 content, which is the result of the lower crystallinity of PE. As the curves also show, the process of thermo-oxidation of pure PE and FAFPs have some exothermic peaks at the temperatures greater than 200°C, two small peaks being in the temperature range of 200–400°C and the major thermal degradation peaks above 400°C. The thermal decomposition of the FAFPs composites revealed several dissociation peaks above 400°C because of the smaller particles of Fe_2O_3.[30] The order of major decomposition temperature of the composites was found as follows, which is in agreement with the TGA results: FAFP3 > FAFP2 > FAFP1 > PE

CONCLUSIONS

In this study, $Fe_2O_3.Al_2O_3$/PE composites with an environmentally benign method were successfully prepared. XRD and FTIR results showed that the particles possess α-Fe_2O_3 and α-Al_2O_3 structure. The SEM-EDX results showed that the dispersion of the Fe_2O_3 particles in the PE matrix is more homogeneous than that of Al_2O_3, because of their smaller particle size.

The thermal stabilities of the composites increased by increasing the Al_2O_3/Fe_2O_3 ratio. The melting temperature increased with an increase in Fe_2O_3 content but the crystallinity decreased. These behaviors are useful for some applications in magnetic and conductive materials, and especially in polymeric catalyst systems that can be used in petrochemical processes.

References

1. Shiyun, L.; Hui, C.; Dongmei, C.; Jianzhong, L.; Zhenjiang, Z.; Yanhui, W.; Tao, T. Polym Compos 2010, 31, 3.
2. Wang, X.; Yun, W. X.; Zhao, B.; Lee; Joong, H.; Prashantha K. Compos Interface 2007, 14, 2.
3. Stoeffler, K.; Lafleun, P. G.; Denault, J. Poly Eng Sci 2008, 48, 12.
4. Merhari, L. Hybrid Nanocomposites for Nanotechnology; Springer: Berlin, 2009; p.827.
5. Pomogailo, A. D.; Kestelman, V. N. Metallopolymer Nanocomposites; Springer: Berlin, 2005; p.563.
6. Aliyeva, R. V. Process Petrochem Oil Refin 2007, 5, 32.
7. Luidi, N.; Carotenuto, G. Metal-Polymer Nanocomposites; John Wiley: New York, 2005.
8. Kozinkin, A. V.; Vlasenko, V. G.; Shuvaev A. T.; Dubovtsev I. A.; Gubin, S. P. Inorg Mater 1996, 32, 376.
9. Pankratov, D. A.; Yurkov, G. Yu.; Kosobudskii, I. D.; Perfilev, Yu. D. In International Conference on Mossbauer Effect: Magnetism, Materials Research, and Gamma-Ray Optics, Kazan, 2000; p.117.
10. Griffiths, G. H.; O'Horo, M. P.; Smith, T. W. J Appl Phys 1979, 50, 7108.
11. Guo, L.; Wu, Z.; Liu, T.; Yang, S. Physica E (Amsterdam) 2000, 8, 199.
12. Zhang, L.; Papaefthymiou, G. C.; Ying, J. Y. J Appl Phys 1997, 81, 6892.
13. Suzdalev, I. P.; Suzdalev, P. I. Usp Khim (Russia) 2001, 70, 203.
14. Rozenberg, A. S. Formation of Ultrafine Particles in Heterogeneous Reactions; Chernogolovka: Institute of Chemical Physics, Russian Academy of Science, 1997; Doctoral Dissertation.
15. Corrias, A.; Ennas, G.; Mountjoy, G.; Paschina, G. Phys Chem 2000, 2, 1045.
16. Vakhshouri, A. R.; Azizov, A.; Aliyeva, R.; Martinova, G.; Quliev, A. J Appl Polym Sci, 2011, 120, 1907.
17. Vakhshouri, A. R.; Aliyeva, R.; Azizov, A.; Gahramanov, N. e-Polym J, submitted.
18. Tadayyon, G.; Zebarjad, S. M.; Sajjadi, S. A. In the Fourth China-Europe Symposium on Processing and Properties of Reinforced Polymers, Guilin, 2009, O-053, 99.
19. Guo, Z.; Zhang, D.; Wei, S.; Wang, Z.; Kraki, A. B.; Li, Y.; Bernazzani, P.; Young, D. P.; Gomes, J. A.; Cocke, D. L.; Ho, T. C. J Nanopart Res 2010, 12, 2415.
20. Kainhofer, R. Available: http://reinhold.kainhofer.com/Physics/Scherrer (accessed May, 2011).
21. Patterson, A. L. Phys Rev Lett 1939, 56, 978.
22. Wu, O. H.; Qu, B. J.; Xu, Y. H.; Wu, Q. Polym Degrad Stab 2000, 68, 97.
23. Xie, R. C.; Qu, B. J.; Hu, K. L. Polym Degrad Stab 2001, 72, 313.
24. Jin, B.; Zhang, W.; Sun, G.; Gu, H. B. J Ceram Process Res 2007, 8, 5, 336.
25. Lee, H. W.; Park, B. K.; Tian, M. Y.; Lee, J. M. J Ind Eng Chem 2006, 12, 295.
26. Hiremath, V. A.; Venkataraman, A. Bull Mater Sci 2003, 26, 391.
27. Zhao, B.; Wang, Y.; Guo, H.; Wang, J.; He, Y.; Jiao, Z.; Wu, M. Mater Sci Poland 2007, 25, 1143.
28. Chen, T.; Cao, Z.; Guo, X.; Nie, J.; Xu, J.; Fan, Z.; Du, B. Polymer 2011, 52, 172.
29. Murty, M. V. S.; Grulke, E. A.; Bhattacharyya, D. Polym Degrad Stab 1998, 61, 421.
30. Wu, R. Y.; Cheng, W.; Wei, J. J Eur Ceram Soc 2000, 20, 67.